Activity report of the Italian CRG beamline at the European Synchrotron Radiation Facility (ESRF)

N 12, Jan 2025
Grenoble, Jan 2025

71 Avenue des Martyrs, Grenoble, France

Editorial manager: Francesco d'Acapito (*dacapito@iom.cnr.it*)
ISSN 2553-9248
DOI: 10.5281/zenodo.14514766

Abstract

This document resumes the activity of the Italian CRG beamline at ESRF (LISA project) during year 2024. The latest news from the beamline are presented as well as details on the technical activity, highlight experiments and publications.

Keywords
Italian beamline at ESRF, BM08
LISA project
X-ray Absorption Spectroscopy

Table of Contents

Foreword ***3***

News from the beamline ***4***

New software **4**

Data reduction 4

Mapping 4

XAS acquisition with full XRF spectra 4

New Sample Holders **5**

Total Electron Yield (TEY) Measurements 5

New sample holder for standard compounds 5

Scientific Highlights ***6***

ReflEXAFS study of metallic nickel using a customized gravity electrochemical cell with laminar flux **6**

Copper-Based Complexes with Adamantane Ring-Conjugated bis(3,5- dimethyl-pyrazol-1-yl)acetate Ligand as Promising Agents for the Treatment of Glioblastoma. **8**

Structure and activity of carbonyl cluster derived PtFe nanoparticles as electrocatalysts for the oxygen reduction reaction in alkaline media **10**

High-entropy alloys investigated by extended X-ray absorption fine structure **12**

Ultrasensitive Luminescence Switching of Zeolite Y Confined Silver Clusters for Dual-Channel Oxygen Sensing **13**

Single Atom Silver-Phosphors in Titanosilicate Matrix for Enhanced LED Applications **15**

Active site formation during pyrolysis of Fe-phthalocyanine derived electrocatalysts for the oxygen reduction reaction **17**

Year 2024 Publications ***19***

Contacts ***21***

Contributors to this issue ***21***

Foreword

The year 2024 has represented a fruitful year LISA, with an intense exploitation of the available beamtime. LISA has provided 471 shifts of beamtime in User Mode, out of which 258 to ESRF users and 213 to CERIC users. In total, 32 experiments have been carried out, 18 in the ESRF quota and 14 in the CERIC quota. The distribution of the scientific areas and the distribution of the Main Proposer (MP) nationalities of the experiments are shown in Figure 1.

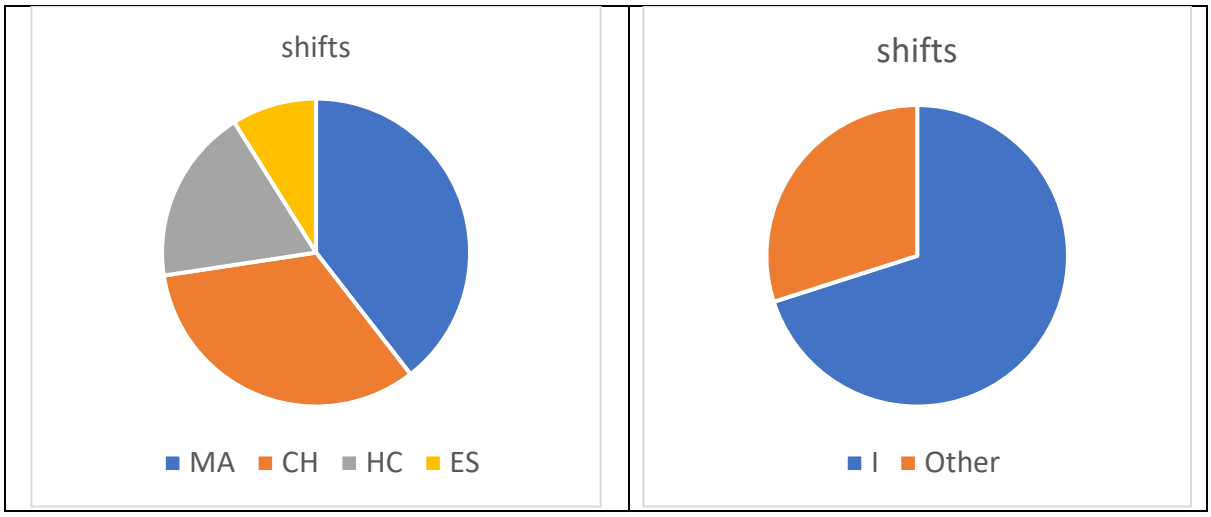

*Figure 1: Statistics on the shifts allocated in 2024 at LISA. **Left**: by Scientific areas **Right**: by nationality of the Main Proposer.*

The most represented scientific areas are Applied Materials Science (MA) and Chemistry (CH) with a lesser contribution from Hard Condensed Matter Science (HC) and Earth Sciences (ES). Cultural heritage studies are present but exclusively in the In-House Research program. Concerning the nationality of the main proposers, Italy has a predominant quota, nonetheless about one third of the beamtime has been dedicated to international users distributed among scientists from Poland, UK, Spain, Germany, France, India. 23 papers related to studies carried out at LISA have been published in 2024 confirming a growing trend since a few years.
For what concerns the ongoing projects it is worth noting the start of the activity of the NEST project (https://fondazionenest.it) with two data collection sessions (with a paper presently under review) and the full start of the CECOMEC project with the recruitment of one post Doc scientist, Dr Simone Amatori. The PON doctorate in collaboration with the Pavia and Milano universities and the De Nora company has continued the activity with new results as reported in the highlight contribution at Page 6.
Concerning teaching and training the LISA staff has hold lectures on XAS to the year 2024 edition of the HERCULES school and ESRF Users Meeting and carried out a one-day lecture on the XAS technique to the students of the Université Grenoble Alpes (M2 – Matière Quantique). In 2024 LISA has hosted a student from the Bologna University, Gabriele Donati, who has worked on the software for the treatment of data collected in fluorescence mode that is described in page 4.

News from the beamline

New software

This year new software has be developed on the beamline to improve the data acquisition and to comply with data fairness and international standard. Accessing at the beamline confluence page you can find all the detailed information.

Data reduction

A new version of the data reduction application, dconv_multiV5, has been released. You can find the whole package at this link in the Zenodo repository. This application not compatible with the old data reduction configuration files. This new tool converts the file in the xdi format, an ascii format developed for the XAS community and read by many XAS tools (i.e. Demeter package and Larch)

Mapping

New tools for map acquisition have been developed, tested and employed at the beamline.
The first tool allows for acquiring map data at fixed energies. The user selects the four corners of the area to analyze, the energy(ies) and the dwell time, then the code will automatically launch and record the maps, with the full fluorescence spectra, transmission, electron and photodiode data.
The second tool converts the 'edf' and 'dat' file obtained from the map acquisition in a single NeXus data file format, and hd5 specifically developed for neutron, x-ray, and muon science.
The final tool is the the map visualyzer which shows and extract the data of the maps, allowing to perform alignment, normalization and subtraction of maps acquired at different energies.

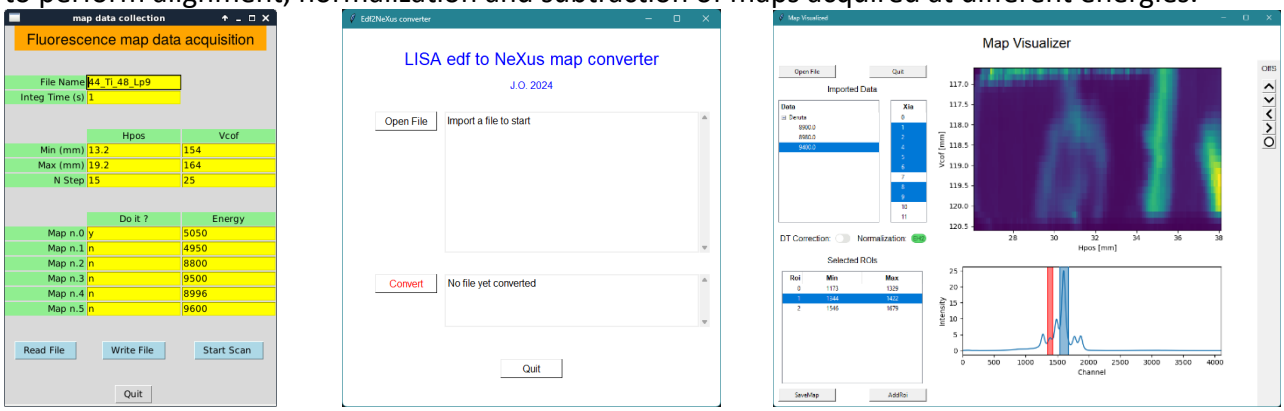

Figure 2 Interfaces of the three mapping tools, on the left the acquisition software, in the center the conversion software and on the right the visualization tool.

XAS acquisition with full XRF spectra

It is now also possible to acquire XAS data recording the full fluorescence spectra. The edf and dat file are then converted to NeXus format for further analysis, here you can download the code and get more info . At the beamline is also present a tool for a-posteriori data extraction using ROI selection on the final NeXus data, chosing also the normalization chamber and the detector dead-time correction. The XAS data are exported directly in the xdi format.

New Sample Holders

Total Electron Yield (TEY) Measurements

A new sample holder has been developed for TEY measurements in collaboration with Institute of Materials Science Leibniz University Hannover, integrating innovative features to enhance performance and ease of use. The holder is made in aluminum and consists of a base and a cover plate, which acts as the cathode, held together by four insulating spacers. The base can host up to 10 specimens mounted on round plates which are clamped to the metallic frame, ensuring an improved electrical contact of the sample to the ground. The cover plate has 10 holes aligned to the samples, to allow the transmission of the X- ray beam.
It is possible to use spacers of different length to adjust the distance from the cover to the sample and accommodate samples of various sizes. The holder can work in vacuum or in controlled atmosphere. Moreover, the holder allows to measure TEY and fluorescence simultaneously by adjusting the incidence angle of the X-ray beam.

Figure 3: left top view of the TEY holder. Right side view of the holder empty and with a sample mounted

New sample holder for standard compounds

A new sample holder made in aluminum for standards or model compounds has been developed in collaboration with Institute of Materials Science Leibniz University Hannover. The holder currently contains the 3d metals from Ti to Zn and is mounted in EH2 behind the measurement chamber. Model compounds are selected moving vertically the holder.

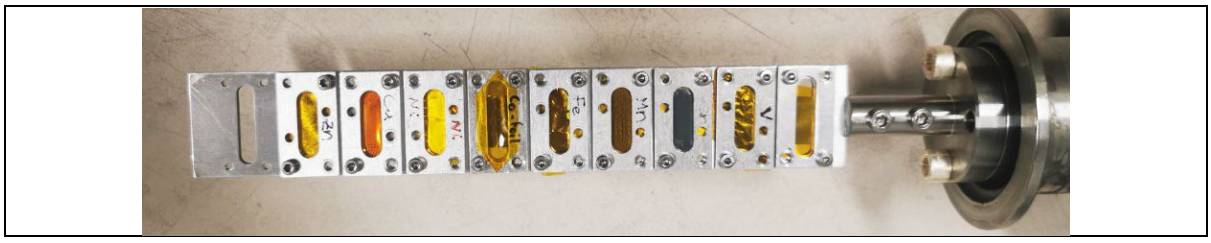

Figure 4: 3d reference metals sample holder with all the elements from Ti to Zn mounted on.

Scientific Highlights

ReflEXAFS study of metallic nickel using a customized gravity electrochemical cell with laminar flux

G. De Amicis[1], F. Panico[2], J. Orsilli[3], A. Testolin[4], F. d'Acapito[3], A. Vertova[2], A. Minguzzi[2], P. Ghigna[1]

[1]Università di Pavia, [2]Università degli Studi di Milano, [3]LISA Beamline, ESRF, [4]Industrie De Nora S.p.A.

This report describes a new strategy for studying electrode materials of industrial interest, like bulk metals or dimensionally stable anodes (DSA®), that possess a relatively low surface-to-bulk atomic ration. To this aim, we designed a novel electrochemical cell for operando grazing incidence X-ray absorption spectroscopy (GI-XAS) studies. The cell must possess the following features: i) being capable of hosting a flat electrode ii) having a thin film of electrolyte in front of the electrode and iii) allow bubbles formed at the electrode to rapidly escape and not influence the XAS spectra.

The cell is made of epoxy resin and allows a laminar layer of electrolyte (here, aqueous 0.1 M KOH) to flow over a bulk electrode by gravity. In this way, the low is perfectly constant and influenced by the pump. Any pulsing in the electrolyte flow would cause a periodic oscillation of the liquid thickness in front of the sample and thus a noise in the final spectra. In this first experiment, we have chosen Ni as the material under investigation, in particular under oxygen evolution reaction (OER).

Figure 5 **(a)** shows the cell design, and setup, while Figure 5 **(b)** presents the cyclic voltammetry (CV) carried out in the potential range 0.9 V to 1.93 V (*vs* RHE) where cathodic (Ni(II)) and anodic (Ni(III)) peaks are visible at about 1.3 V and 1.4 V (*vs* RHE), respectively. These results guided the selection of potential values, marked by arrows, at the XAS spectra were recorded.

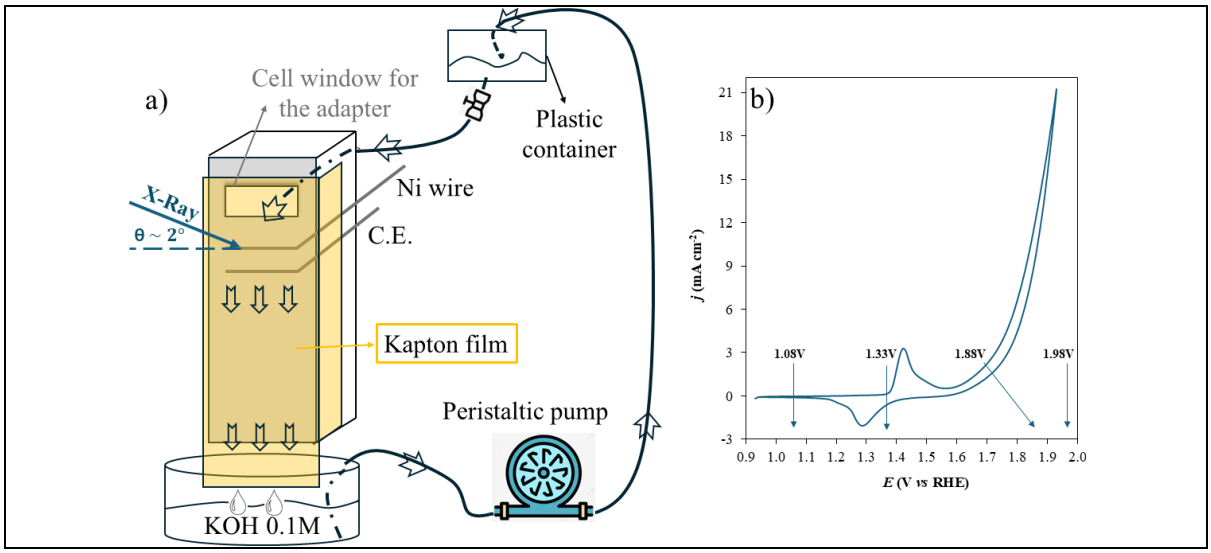

*Figure 5: Design and setup of the "gravity" electrochemical cell. **(b)** Cyclic voltammetry of Ni wire recorded in the "gravity" cell at 0.05 V s^{-1} in 0.1 M KOH.*

The W.E. and the C.E. were Ni wire electrodes, while the R.E. was an Ag/AgCl (in 3 M KCl).

A Kapton film was placed over the cell to stabilize the electrolyte thickness, prevent water trickles, and ensure complete electrode surface coverage.

To demonstrate the surface sensitivity of the setup, spectra recorded at 1.33 V were compared using GI and GE (grazing emission) geometries. The comparison of the Ni/NiO/NiOOH standard spectra (Figure 6 **A**) with the spectra show Figure 6**B** allow to state that the GE

configuration is more sensitive to the bulk than the GI, the latter showing a clear peak at ca. 8347 eV, consistent with the presence of surface NiO.

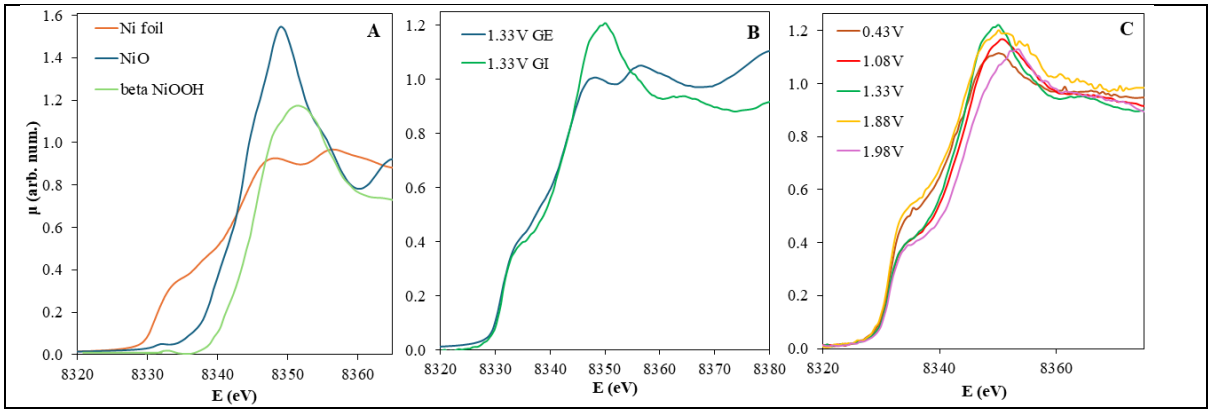

Figure 6: Ni K-edge XANES in A) the spectra of Ni foil, NiO and β-NiOOH are shown as reference of the edge position of Ni(0), Ni(II) and Ni(III). In B) the comparison of the spectra recording at 1.33 V with GI and GE. In C) XANES spectra under operando conditions recorded at different potentials with GI geometry.

For what concerns the study at different applied potentials, Figure 6**C**, it is worth noting that all the spectra are consistent with the presence of some metallic Ni, evidenced by the shoulder at ca. 8333 eV, plus some oxidized Ni, which is detected by peaks centered between ca. 8350 and 8354 eV. Below 1.88 V, the energy position of the main peak is ca. 8350 eV, which is consistent with the presence of NiO. At 1.98 V, and this peak shifts towards higher energies, likely demonstrating the formation of Ni(III), as confirmed by comparison with the spectra of the standards shown in Figure 6 **A**. In more detail, at 1.88 V the presence of both Ni(II) and Ni(III) is detected, as indicated by the large and double-maximum peak. At highest anodic potential, 1.98 V, the spectrum is indicative of the presence of Ni(III) only, as evidenced by the peak shifting to the 8350 eV. Conversely, in the spectrum at 0.43 V, only Ni(II) is present. The presence of metallic Ni contribution in all spectra may be attributed to the unavoidable presence of scattered photons by the electrolyte, which impinge on the sample at random angles, and therefore probe also the electrode bulk. In addition, the spectra appear to be quite somewhat affected by self-absorption effects, making a quantitative analysis difficult.

Publication: [Journal of Synchrotron Radiation - *Submitted*]

Copper-Based Complexes with Adamantane Ring-Conjugated bis(3,5- dimethyl-pyrazol-1-yl)acetate Ligand as Promising Agents for the Treatment of Glioblastoma.

M. B. Morelli[a], M. Caviglia[b], C. Santini[b], J. Del Gobbo[b], L. Zeppa[a], F. Del Bello[a], G. Giorgioni[a], A. Piergentili[a], W. Quaglia[a], C. Battocchio[c], F. Bertel[c], S. Amatori[c], C. Meneghini[c], G. Iucci[c], I. Venditti[c], A. Dolmella[d], M. Di Palma[e], and M. Pellei[b].
a) School of Pharmacy, University of Camerino, Italy.
b) School of Science and Technology, University of Camerino, Italy.
c) Department of Science, Roma Tre University, Italy.
d) Department of Pharmaceutical and Pharmacological Sciences, University of Padova, Italy.
e) Department of Biomedical Sciences, University of Padova, Italy.

Copper is one of the essential trace metals for all organisms living in oxygen rich environments. It plays a crucial role in several different processes within the cell and it's currently under investigation for its antitumoral properties against various kinds of solid tumors. This interest comes from the need to find substitutes for a number of already commercially available metal-based drugs such as cisplatin, that, despite its efficacy in tumor treatment, suffers from a number of limitations such as the acquired resistance and the inherent cumulative toxicity. Our recent studies on potential anticancer Cu(I) and Cu(II) complexes supported by functionalized bis(pyrazol-1-yl)acetates helped to demonstrate that a proper coordination improves the bioavailability and the cellular uptake of the complexes, as well as significant cytotoxic effects against different human tumor cell lines. In this study the bis(3,5-dimethyl-pyrazol-1-yl)acetic acid, conjugated to the known drug amantadine, has been used as a chelator for the synthesis of the new Cu(I) and Cu(II) complexes 1-5 (Figure 7) to be evaluated as potential agents for the treatment of glioblastoma. Amantadine was selected as a bioactive molecule since it has recently demonstrated to show from moderate to good antiproliferative effects in different human tumor cell lines.

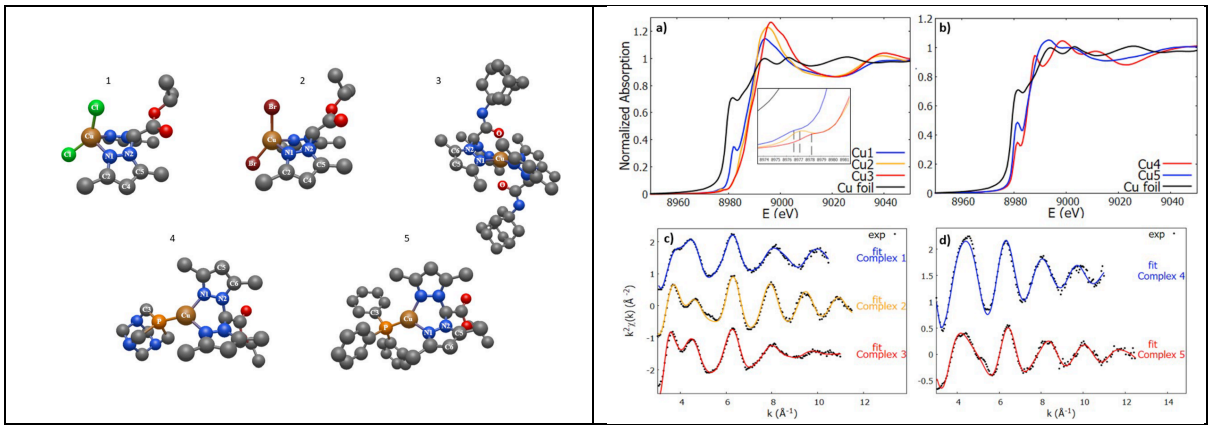

Figure 7: (left) DFT-optimized models for Cu(II) (1, 2 and 3) and Cu(I) (4 and 5) *(left) DFT-optimized models for Cu(II) (1, 2 and 3) and Cu(I) (4 and 5) coordination compounds. The neighbors involved in the most intense single and multiple scattering paths are highlighted in the image. (right) (a, b) Cu K edge and XANES region for Cu(II) and Cu(I) complexes (inset highlights the pre-edge region peaks). Comparison between experimental and fit in K space for Cu(II) complexes (c) and Cu(I) (d).*

The structures of the copper complexes were investigated by X-ray absorption spectroscopy (XAS) as well as complementary techniques and tested with different glioblastoma cells allowing to correlate their Cu coordination with their antitumoral and antiproliferative properties. Among the investigated complexes, 3 and 5 significantly decreased cell viability, affecting cell growth, proliferation, and death. The Cu K edge XAS measurements were carried out at the European Synchrotron Radiation Facility (ESRF), on beamline BM08 on the Cu(II) (1-

3) and Cu(I) (4 and 5) complexes with the aim of describing their average valence state, coordination chemistry, and local atomic structure around the absorber by probing both the near edge (XANES) and extended (EXAFS) regions of the spectrum. The normalized Cu XANES spectra of complexes 1, 2, and 3 indicate distinct Cu(II) oxidation states with different geometries. Complex 1, in a square planar geometry, exhibits an intense 1s→4p transition peak at 8984 eV, which is absent in complexes 2 and 3. Complex 2 (tetrahedral) and complex 3 (octahedral) show weak 1s→3d transitions, with differences attributed to geometric configurations and hybridization effects. In contrast, Cu(I) complexes 4 and 5 display no pre-edge peaks and a strong 1s→4p transition around 8982 eV, the edge position and shape being consistent with Cu(I) valence states in a trigonal planar geometry. Complex 4 presents an additional post-edge peak, suggesting localized distortions that result in a T-shaped configuration rather than a perfect trigonal planar structure. Quantitative analysis of the EXAFS signals was achieved by fitting the k2-weighted theoretical curves k2χth to the raw experimental data k2χexp. The theoretical curve χt h(k) was calculated as a sum of partial contributions, using the standard EXAFS formula and Gaussian disorder approximation. The photoelectron scattering amplitudes and phase functions were calculated using the FEFF8 software on optimized DFT atomic model of the complexes. For each sample, the relevant single (SS) and multiple scattering (MS) contributions to the EXAFS signal were identified and a trial-and-error procedure was performed to minimize the number of free variables. All samples show a common bis(pyrazol-1-yl) bidentate moiety in the local environment of copper ions. Additionally, complexes 1 and 2 show the characteristic signals of the halogen neighboring atoms Cu−Cl and Cu−Br, while complex 3 shows the Cu−O scattering path from the apical oxygen atoms, as well as multiplicities coherent with two bis(pyrazol-1-yl) fragments in the plane of the octahedron. Complexes 4 and 5 also show signals coming from their phosphane co-ligands, PTA and PPh3 respectively. The EXAFS data analysis, which confirms the goodness of the DFT model, allows to further improve our knowledge of the Cu coordination parameters in these complexes.

Publication: M. B. Morelli, M. Caviglia, C. Santini, J. Del Gobbo, L. Zeppa, F. Del Bello, G. Giorgioni, A. Piergentili, W. Quaglia, C. Battocchio, F. Bertel., S. Amatori, C. Meneghini, G. Iucci, I. Venditti, A. Dolmella, M. Di Palma and M. Pellei; J. Med. Chem. 2024, 67, 9662-9685.

Structure and activity of carbonyl cluster derived PtFe nanoparticles as electrocatalysts for the oxygen reduction reaction in alkaline media

Xiufang He[1], Martina Fracchia[2,3], Mauro Coduri[2,3], Marco Scavin[1,3], Paolo Ghigna[2,3], Marcello Marelli[6], Roberto della Pergol1a[5], Alberto Vertova[1,3], Alessandro Minguzzi[1,3,4]*

1 Dipartimento di Chimica, Università degli Studi di Milano, Via Golgi 19, 20133, Milan, Italy

2 Dipartimento di Chimica, Università degli Studi di Pavia, Viale Taramelli 13, 27100, Pavia, Italy

3 INSTM, National Inter-University Consortium for Materials Science and Technology, Via G. Giusti 9, 50121 Florence, Italy

4 Dipartimento di Energia, Politecnico di Milano, Via Lambruschini, 4a - 20156 Milano, Italy

5 Dipartimento di Scienze dell'ambiente e della Terra, Università degli Studi di Milano-Bicocca, Piazza della Scienza 1, 20126 Milano, Italy

6CNR SCITEC - Istituto di Scienze e Tecnologie Chimiche "Giulio Natta", Via Fantoli 16/15, 20138 Milano

Developing low-content Pt-based cathodic electrodes remains a critical focus for addressing the challenges of slow kinetics in the oxygen reduction reaction (ORR). In this work, PtFe nanoparticles derived from carbonyl clusters were prepared. In order to tailor their surface composition and morphology, part of the nanoparticles was and thermally treated at 180 °C under hydrogen, which was named as PtFe_H_2, and the untreated sample was named as PtFe_UN. The resulting materials was analysed through X-ray absorption spectroscopy (XAS) to investigate the local structure and electronic properties.

X-ray absorption spectra were collected at the Pt L_3-edge (11564 eV) and Fe K-edge (7112 eV) in transmission or fluorescence mode at the LISA beamline of the ESRF. A Si (311) double crystal monochromator was employed for the Pt L_3-edge, while a Si(111) double crystal monochromator was utilized for the Fe K-edge. Harmonic suppression below 20 keV was achieved using Pd-coated mirrors[1]. In the measurement, Pt foil, Fe foil was used to calibrate the energy. The spectra of Pt/C and α-FeOOH were acquired as the reference. X-ray data were analysed using the ATHENA software, part of the IFEFFIT package [2].

The Pt L_3-edge spectra are presented in Figure 8**a**. The primary intensity peak, known as the White Line (WL), located around 11568 eV, which is corresponding to transitions from filled $2p_{3/2}$ orbitals to empty 5d orbitals. This peak is notably intense for PtFe_UN, especially in comparison to the Pt foil spectrum. This observation aligns well with the behaviour that PtFe samples undergo particle oxidation when they were exposed to air. As a consequence, the electron density on Pt atoms were reduced by bonding with light elements, such as O, C as well as alloying with Fe[3]. However, the WL intensity of PtFe_H_2 is lower than that of PtFe_UN, indicating the lower surface oxidation and larger nanoparticle size of PtFe_H_2 in comparison with PtFe_UN. It is likely that the H_2 treatment eliminated some Pt-C and Pt-O bonds, resulting in a material with greater crystallinity and a higher proportion of metallic Pt compared to PtFe_UN.

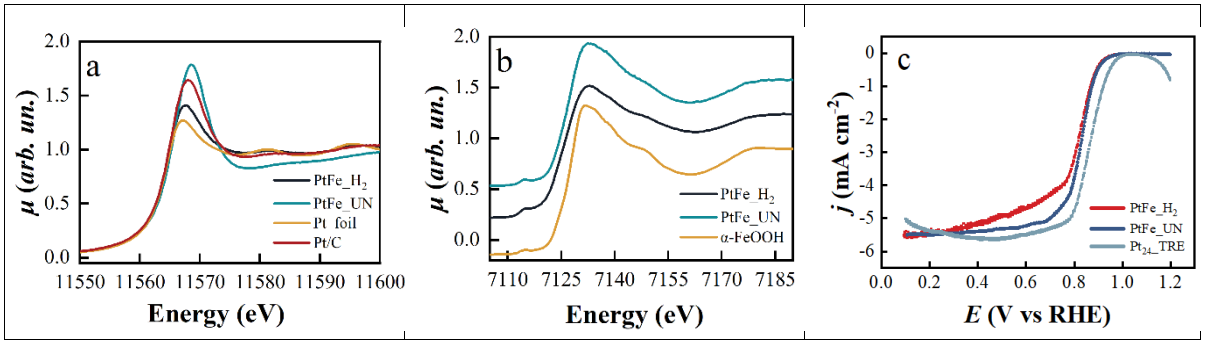

Figure 8: (a) XANES spectra recorded at the Pt L3-edge of PtFe_H2, PtFe_UN, Pt foil and Pt/C. (b) XANES spectra recorded at the Fe K-edge of PtFe_H2 and PtFe_UN. The spectrum of α-FeOOH has also been reported for comparison. (c) the 3rd CV half-cycle recorded in in O_2-saturated 0.1 M KOH solution at 20mV·s-1, at 1600 RPM. (Reprinted with permission from ACS Appl. Energy Mater., 2024, 7 (4), 1561–1572. Copyright 2024 American Chemical Society.)

To investigate the local environment of iron in the PtFe nanoparticles, XAS spectra were also recorded at the Fe K-edge (Figure 8**b**). It is evident that the shape and energy position of the PtFe samples are almost identical to those of α-FeOOH, indicating that the iron in these samples is primarily in an oxidized state, nearly to be 2[4]. In contrast, the spectrum of PtFe_H_2 shows a noticeable shift to the left, suggesting a reduction of iron to the metallic state. This shift indicates a decrease in the oxidation state of iron, likely due to the thermal treatment under hydrogen, which effectively removes some of the oxygen from the iron atoms. This is consistent with the findings from the Pt L_3-edge, where a lower level of oxidation was observed in the PtFe_H_2 sample compared to PtFe_UN. The onset potential of the synthesized samples is shown in Figure 8**c**. It is evident that PtFe_UN reaches the diffusion regime more quickly than PtFe_H_2, leading to enhanced electrocatalytic activity. We propose that the thermal treatment under H_2 affects the surface properties of the Vulcan support, making it primarily hydrophobic after treatment. This suggests that the surface modifications of the support material have a significant impact on the overall catalytic behaviour of the PtFe nanoparticles.

Publication: [ACS Applied Energy Materials 7 (2024), 1561-1572]

Reference

1. D'Acapito, F. et al. J Synchrotron Radiat 26, 551–558 (2019).
2. Ravel, B. & Newville, M. J Synchrotron Radiat 12, 537–541 (2005).
3. Morris, D. J. & Zhang, P. Chemistry–Methods 1, 162–172 (2021).
4. Fracchia, M. et al. ACS Appl Energy Mater 1, 1716–1725 (2018).

High-entropy alloys investigated by extended X-ray absorption fine structure

A. Fantin[1,2]

[1]BAM Berlin, [2]HZ Berlin

Alloys composed of multiple components, often referred to as High-Entropy Alloys (HEAs), derive their stability from high configurational entropy (S). This entropy S, by outweighing the formation enthalpy (H), reduces the overall Gibbs energy (G = H - TS, where T represents temperature), thereby stabilizing the crystal structure of the alloy. Since mechanical properties are largely influenced by atomic interactions within the solid solution phase, as well as between the solid solution and any segregated intermetallic phases, investigating atomic-level phenomena — such as site preferences, chemical short-range ordering (CSRO), and local lattice distortions (LLD) — is essential. Extended X-ray absorption spectroscopy (EXAFS) carried out at LISA-BM08 beamline (CRG-ESRF) allowed over the years investigations on different alloys, resulting in several papers published on *fcc*-based [1-3] systems and on one topologically close packed σ-phase [4]. Because of rarely available literature on experimentally determined CSRO and LLD on *bcc*-based High-Entropy alloy systems, EXAFS measurements at LISA-BM08 were carried out on an equiatomic *bcc* MoNbTaW, with results published in [5]

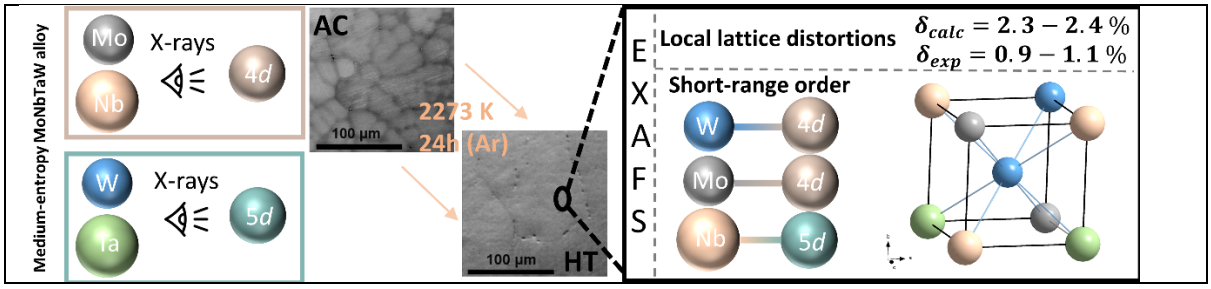

Figure 9: Graphical abstract evidencing the low scattering contrast between 4d elements (Mo, Nb) and 5d elements (W, Ta) against X-rays, the As-cast (AC) microstructure changes after the homogenization treatment (HT), and the EXAFS results on local lattice lattice distortions and chemical short-range ordering measured on the annealed MoNbTaW [5].

Small 1st and 2nd shell element-specific lattice distortions were unexpectedly found, as it is often mentioned in literature that HEAs carry larger lattice distortions than conventional alloys, especially in *bcc* structures. The experimental size-mismatch parameter, δ_{exp}, is determined to be ca. 50% lower than the corresponding calculated value based on metallic radii considerations. Around W, CSRO preferring 4*d* elements in the 1st and 2nd shells persists, which, combined with simulation data on the same system available in literature, points to W-Nb ordering [Figure 9]. Such preference in the solid-solution is reminiscent of atomic site-preferences in lower temperatures phases such as in the B2(Mo,W;Ta,Nb)- and the B32(Nb,W)-phases. As previously demonstrated for *fcc* phases [1-3], high-temperature (i.e. solid solution) ordering preferences seem foreshadowing low-temperature phase formation, suggesting a general feature of high-temperature CSRO.

***Publications**: [1] Small Sci. **4**(2) (2024), 2300225. [2] Mat. Chem. Phys **276** (2022), 125432 [3] Acta Mat. **193** (2020), 329-337. [4] Acta Mat. **259** (2023), 119277. [5] Mat. Res. Lett. **12**(5) (2024), 346-354.*

Ultrasensitive Luminescence Switching of Zeolite Y Confined Silver Clusters for Dual-Channel Oxygen Sensing

Li Sun[1], G. Romolini[1], B. Dieu[1], D. Grandjean[2], M. Keshavarz[3], E. Fron[4], F.o D'Acapito[5], M. B. J. Roeffaers[6], M. Van der Auweraer[1] and J. Hofkens[1,7*]*

[1] Department of Chemistry KU Leuven, Belgium, [2] Department of Physics and Astronomy, KU Leuven, Belgium, [3] Department of Electrical Engineering KU Leuven, Belgium, [4] KU Leuven Core facility for Advanced Spectroscopy, Belgium, [5] CNR-IOM-OGG, c/o ESRF, LISA CRG, France, [6] Department of Microbial and Molecular Systems, KU Leuven, Belgium, [7] Max Planck Institute for Polymer Research, Germany.

This work introduces an innovative oxygen-sensing material based on silver clusters confined within Faujasite Y (FAU-Y) zeolites. Silver clusters formed through a simple ion-exchange and thermal activation process demonstrate a photoluminescence quantum yield (PLQY) of 31% and a long luminescence lifetime of 541 µs. These clusters offer dual-channel sensing via emission quenching and lifetime reduction, achieving ultrasensitive oxygen detection with a detection limit of 58 Pa and response times under 1 second.

The silver-exchanged lithium FAU-Y (AgLiY) zeolite was prepared via ion exchange and thermal activation at 450 °C. Subsequently, hydrogen treatment produced luminescent silver clusters. Initially, the material exhibited weak blue-green emission under UV light. However, hydrogenation introduced a prominent orange emission centered at 610 nm. The emission was reversible under air/vacuum switching, indicating its suitability for oxygen-sensing applications. The orange emission showed a decay time of 541 µs and a PLQY of 31%, significantly outperforming comparable systems.

The material's performance stems from its structural properties and interactions with oxygen, both elucidated through advanced spectroscopic and structural characterization techniques. Extended X-ray Absorption Fine Structure (EXAFS) analysis was instrumental in understanding the local atomic environment of the silver clusters, providing insights into the structural origin of their luminescent properties and dynamic quenching behavior.

EXAFS, coupled with X-ray excited optical luminescence (XEOL), provided detailed insights into the atomic-scale structure of the luminescent silver clusters. Phase-corrected Fourier Transform (FT) analysis of EXAFS data revealed two main coordination environments for the silver atoms: The Ag–Ag distances within the clusters were measured at 2.87 Å, consistent with a bicapped tetrahedral structure (Ag_6). Surrounding the clusters were on average 2.1 oxygen atoms at 2.42 Å and 2.6 lithium ions at 2.93 Å, indicating interactions with the zeolite framework and confined water molecules.

The analysis confirmed that the material consists of a mixture of Ag_4^{x+} and Ag_6^{y+} clusters, with the latter responsible for the orange emission. The Ag_6^{y+} was identified as the primary orange luminescent species, located within the sodalite cages of the zeolite framework. This is the first report of such clusters in FAU-Y zeolites, marking a significant advancement in the field of silver-cluster-based luminescent materials.

The oxygen-sensing mechanism relies on dynamic (collisional) quenching of the excited Ag_6^{y+} by O_2. Upon exposure to oxygen, the orange emission is quenched due to energy transfer processes that reduce the excited-state lifetime. Stern-Volmer plots for both intensity and lifetime quenching showed linear behavior over a wide oxygen concentration range (0–100 kPa), confirming a dynamic quenching mechanism. The experimentally determined quenching rate constants were significantly lower than those expected for a diffusion-

controlled process, suggesting restricted orbital overlap between oxygen and the clusters due to the zeolite's spatial constraints.

In conclusion, the integration of advanced spectroscopic techniques like EXAFS with innovative material design has paved the way for next-generation optical sensors, offering unmatched performance and versatility in gas detection technologies.

This study highlights the power of EXAFS in elucidating the structural basis of functional nanomaterials [Figure 10]. The Ag_6^{y+}confined in FAU-Y zeolites represent a breakthrough in oxygen sensing, combining high sensitivity, fast response, and excellent stability. Beyond oxygen sensing, the findings open avenues for exploring other metal-cluster-based zeolite systems for applications in gas sensing, imaging, and optoelectronic devices. Overall, we demonstrated that the sensor achieves a detection limit of 58 Pa, and the luminescence switching is reversible under air/vacuum cycling, with the material retaining its structural integrity and optical properties even after prolonged use. The response times are less than 1 second, attributed to the efficient diffusion of oxygen within the zeolite framework. EXAFS and powder X-ray diffraction confirmed the stability of the AgLiY structure, even after repeated sensing cycles and one year of storage.

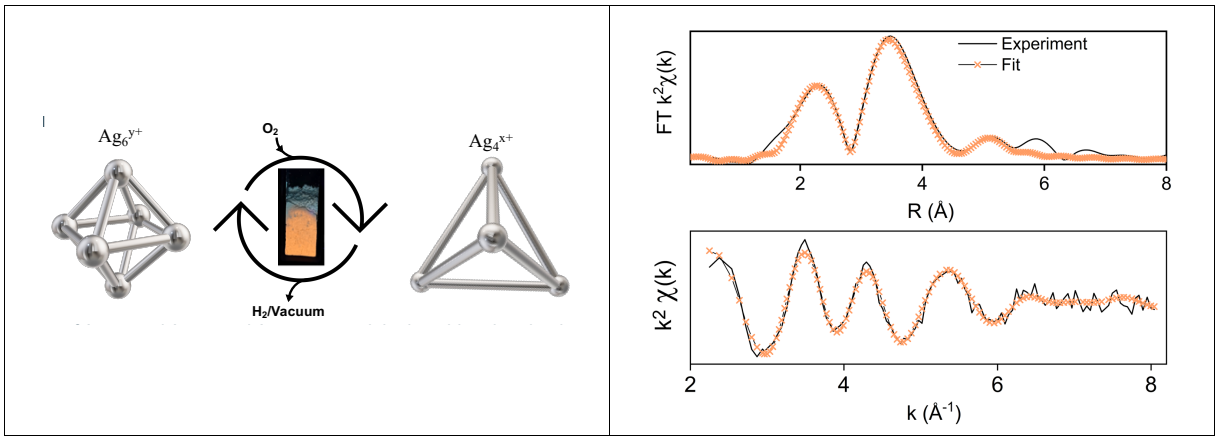

Figure 10: Left: Schematic representation of the conversion mechanism between Ag6y+and Ag4x+. At the center of the circle is a picture of Ag-FAU-Y under UV light. The orange luminescence is at the bottom of the cuvette where air did not diffuse yet, the blue/green luminescence comes from the top of the same cuvette already exposed to air. ***Right****: FT XEOL-EXAFS k2-weigthed (top), XEOL-EXAFS (bottom) of Ag-FAU-Y.*

Publication: L. Sun, G. Romolini, B. Dieu, D. Grandjean, M. Keshavarz, E. Fron, F. D'Acapito, M. B. J. Roeffaers, M. Van der Auweraer, J. Hofkens, *Advanced Optical Materials* **2024**, *12*, 2400784.

Single Atom Silver-Phosphors in Titanosilicate Matrix for Enhanced LED Applications

G. Romolini[1], L. Sun[1], E. Fron[1,2], F. d'Acapito[3], D. Grandjean[4], M. B. J. Roeffaers[5], C. Martin[6], J. Hofkens[1,7]**

[1] Department of Chemistry KU Leuven, Belgium, [2] KU Leuven Core facility for Advanced Spectroscopy, Belgium, [3] CNR-IOM-OGG, c/o ESRF, LISA CRG, France, [4] Department of Physics and Astronomy, KU Leuven, Belgium, [5] Department of Microbial and Molecular Systems, KU Leuven, Belgium, [6] Department of Physical Chemistry, University of Castilla-La Mancha, Spain, [7] Max Planck Institute for Polymer Research, Germany.

Small metal clusters, such as silver species, are highly interesting for their exceptional optoelectronic properties and wide-range applications, varying from sensing and imaging to catalysis. However, their use in light-emitting devices (LEDs) is limited by their instability and tendency to grow into larger metallic particles; thus, requiring stabilizing matrices like zeolites or silica. Unfortunately, these matrices often exhibit low electrical conductivity, reducing their efficacy in electronic applications. This study proposes a microporous titanosilicate (TiSi) as a semiconducting stabilizer for Ag-based materials, offering a promising solution to the mentioned challenges, as TiSi scaffolds combine high thermochemical stability with intrinsic semiconducting properties, making them ideal for stabilizing luminescent silver species.

After exchange of Na^+ ions with Ag^+, and thermal treatment, optical spectroscopy revealed that silver exchanged titanosilicate (Ag-TiSi) exhibits bright orange fluorescence with a photoluminescence quantum yield of 20%, see **Figure 11 left**. To pinpoint the origin of the new optical properties, advanced structural characterization through X-ray absorption spectroscopy, performed at the LISA beamline at the ESRF, was conducted to elucidate the electronic and atomic-scale properties of Ag species embedded within the matrix. X-ray absorption near edge spectroscopy (XANES) provided bulk-level insights demonstrating that the lowest-loaded sample exhibits a pronounced first oscillation after the white line (~25,535 eV), indicative of higher local order and limited static disorder.

Tr-EXAFS provided a comprehensive view of dark and luminescent species, while XEOL-EXAFS specifically targeted luminescent centers, see Figure 11 for experimental data and corresponding fits. For the lowest loading of silver, single Ag^+ was found to occupy the Na^+ positions present on the non-exchanged TiSi, accompanied by significant structural distortions. The analysis of Tr-EXAFS signal revealed that Ag cations are surrounded by on average 3.8 oxygen atoms (2.27 Å), 1.9 Si atoms (2.92–2.97 Å), and 4 Ti atoms (3.74–3.77 Å). The high Debye–Waller factors observed for Ag-Si contributions, particularly at higher Ag loadings, suggest increasing static disorder with a corresponding distortion of the TiSi framework.

Finally, XEOL-EXAFS confirmed the presence of single Ag^+ as luminescent centers, with slightly shorter Ag-Si distances compared to Tr-EXAFS results, reflecting a greater distortion of the Ag site. These observations align with complementary findings from Rietveld refinement against powder diffraction data under hydrated and dehydrated conditions. While discrepancies in Ag-O distances were observed, they likely arise from sample dehydration under the synchrotron high X-ray flux, a factor mitigated when collecting powder X-ray diffraction in the lab.

To evaluate the electroluminescent properties of Ag-TiSi, the material was integrated as an emissive layer within a proof-of-concept LED. The resulting device demonstrated a low turn-on voltage of 2 V and a high colour rendering index of 80, showcasing significant improvements over traditional Silver Zeolite composite based LEDs (ZEOLED).[1,2] This work

highlights the potential of titanosilicate-stabilized Ag^+ as advanced luminescent materials for energy-efficient LEDs and other optoelectronic applications.

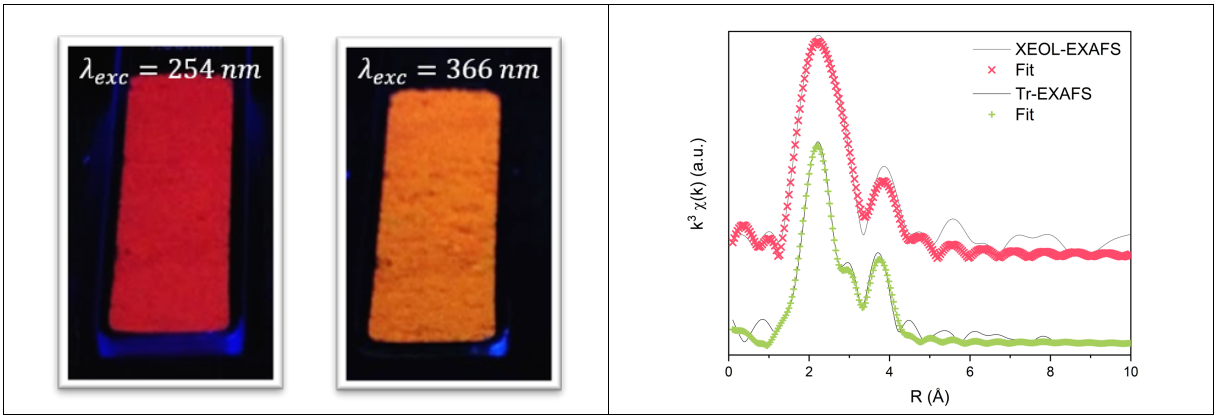

Figure 11: Left: Picture of Ag-TiSi under UV light, after ion-exchange with Ag+ and after thermal activation at 450 °C. Right: Phase-corrected FT of both XEOL- and Tr-EXAFS (black solid line) and corresponding fits (crosses) of Ag-TiSi with lowest Ag+ loading, corresponding to the most luminescent sample.

Publication: G. Romolini, L. Sun, E. Fron, F. d'Acapito, D. Grandjean, M.B.J. Roeffaers, C. Martìn, J. Hofkens, *Advanced Optical Materials* **2023**, 202301894.

[1] K. Kennes, C. Martin, W. Baekelant, E. Coutino-Gonzalez, E. Fron, M. B. J. Roeffaers, J. Hofkens, M. Van Der Auweraer, *ACS Appl. Mater. Interfaces* **2019**, *11*, 12179.

[2] K. Kennes, E. Coutino-Gonzalez, C. Martin, W. Baekelant, M. B. J. Roeffaers, M. Van der Auweraer, *Advanced Functional Materials* **2017**, *27*, 1606411.

Active site formation during pyrolysis of Fe-phthalocyanine derived electrocatalysts for the oxygen reduction reaction

M. Muhyuddin[1], E. Berretti[2], J. Orsilli[1,3], R. Lorenzi[1], F. D'Acapito[3], P. Atanassov[4], A. Lavacchi[2], C. Santoro[1]

[1]University of Milano-Bicocca; [2]Istituto di Chimica Dei Composti Organo Metallici (ICCOM), Consiglio Nazionale Delle Ricerche (CNR); [3]CNR-IOM-OGG, c/o ESRF LISA CRG, [4]University of California Irvine

Iron-based atomically dispersed metal-nitrogen-carbon (Fe-Nx-Cs) electrocatalysts emerging as a promising solution to replace platinum for the oxygen reduction reaction. These Fe-Nx-Cs are made from earth-abundant materials and mimic natural enzymes, offering high ORR activity, especially in alkaline media. The performance of these electrocatalysts is strongly influenced by the pyrolysis process, which is essential for developing the active sites in Fe-Nx-Cs. Pyrolysis, a thermal process that occurs in an oxygen-free environment, is crucial for creating homogeneously dispersed active sites at the atomic level. However, the exact mechanisms of pyrolysis and its impact on the electrocatalyst performance remain poorly understood, with ongoing research focusing on optimizing the pyrolysis conditions.
Recent studies have highlighted the role of pyrolysis temperature, atmosphere, and ramp rate in determining the activity of Fe-Nx-Cs. For example, variations in the pyrolysis atmosphere and temperature can lead to different nitrogen-based moieties and iron coordination structures, influencing ORR performance. In particular, iron's coordination with nitrogen (Fe-Nx) and its interaction with other atoms during pyrolysis are key factors in determining the electrocatalytic efficiency. Despite significant progress, the complex interplay of these factors has not been fully elucidated.
In this context, a study focused on Fe-Nx-Cs synthesized from iron (II) phthalocyanine (FePc) mixed with a carbon matrix (Ketjen Black 600) investigates how different pyrolysis conditions (temperature and atmosphere) affect the iron active site formation and its evolution. Using techniques such as in-situ and ex-situ X-ray absorption spectroscopy (XAS), the study intended to examine how the speciation of iron changes during pyrolysis and correlates these changes with electrocatalytic performance in the ORR. Pyrolysis temperatures (200°C–1000°C) and pyrolysis atmospheres (argon and argon/hydrogen) were varied and the impact on the evolution of Fe-based moieties, thus contributing to the electrocatalytic properties of the electrocatalysts.
The pyrolytic conditions have an important influence on the iron speciation. In fact, the study reveals that pyrolysis at temperatures above 600°C induces significant phase transitions in the Fe-Nx-Cs structure. Below this threshold, the iron coordination in Fe-Nx moieties remains relatively stable, with minor rearrangements observed. However, beyond 600°C, there is a clear transformation from a single-atom Fe-Nx configuration to metallic iron and magnetite, with distinct effects depending on the pyrolytic atmosphere investigated based on Ar (neutral atmosphere) vs. slightly reducing (Ar/H_2).
Ex situ and in-situ XAS measurements were conducted to evaluate the iron speciation during pyrolysis. A specific microtome cell was designed for this experiment as shown in Figure 12 a and b. In situ XANES spectra show that the coordination of Fe undergoes significant changes during pyrolysis, especially above 600°C (Figure 12 c and d). Notably, the pre-edge features, indicative of Fe-Nx coordination, start to diminish and completely vanish at 500°C, which is associated with the desorption of oxygen and the transformation of the Fe coordination from pyramidal to planar geometry (**Error! Reference source not found.**c and d). The recovery of initial features when exposed to air points to the reversible nature of oxygen adsorption on the iron sites, resembling the behaviour of natural enzymes like hemoglobin.

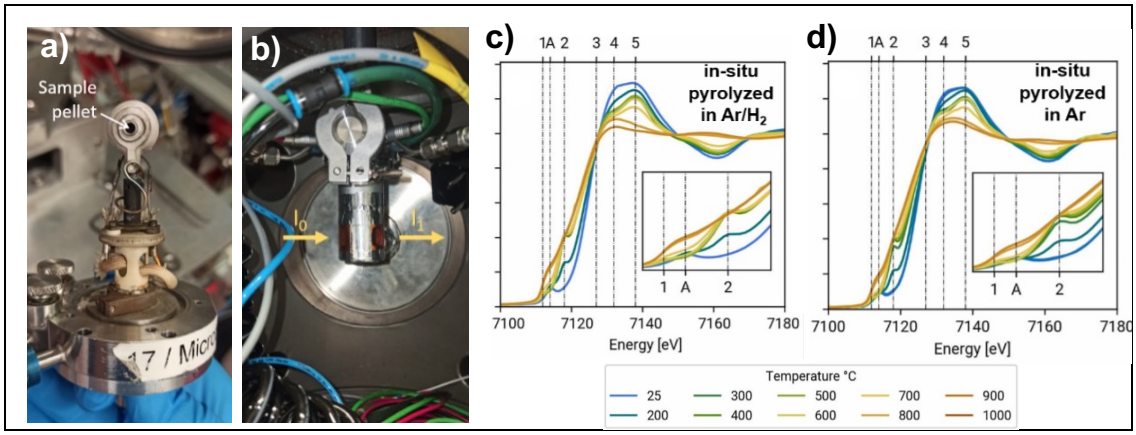

Figure 12: Figure 1 a-b) Microtome cell set up; c) XANES of the FePc functionalized carbon in Ar/H2 atmosphere and d) Ar atmosphere. Figures c and d were arranged from Appl. Catal. B: Environ. 343, 2024, 123515, Elsevier, Copyright 2024. Licensed under CC-BY 4.0

Linear combination fitting (LCF) of EXAFS spectra indicates the reduction of FePc active sites and the formation of α-Fe, γ-Fe, and magnetite as the temperature increases probably due to the agglomeration of the metallic sites. Importantly, the optimal electrocatalytic activity for ORR was found at 600°C, where Fe-Nx-C single-atom configurations were still present. Beyond this temperature, as metallic phases began to dominate, electrocatalytic activity decreased. This reinforces the importance of maintaining single-atom Fe-Nx species for efficient electrocatalysis.

The findings suggest that by carefully controlling the pyrolysis conditions, it is possible to optimize the active site configuration and enhance the performance of Fe-Nx-Cs for sustainable energy production. This methodology could be applied more broadly to other electrochemical reactions and types of electrocatalysts.

Overall, this research underscores the importance of understanding the pyrolysis process to improve the development of cost-effective and efficient electrocatalysts, contributing to the commercialization of hydrogen fuel cells and other clean energy technologies.

Publication : Appl. Catal. B: Environ. 343, 2024, 123515

Year 2024 Publications

1) Amthor S., Ranu K., Bellido C.G., Salomón F.F., Piccioni A., Mazzaro R., Boscherini F., Pasquini L., Gil-Sepulcre M., Llobet A. - Robust molecular anodes for electrocatalytic water oxidation based on electropolymerized molecular Cu complexes Advanced Materials 36, 2308392-1-2308392-7(2024)
2) Berretti E., Giaccherini A., Dell'Aquila V., Di Benedetto F., Montegrossi G., Lepore G.O., Innocenti M., d'Acapito F., Vizza F., Lavacchi A. - In-situ and operando Grazing Incidence XAS: a novel set-up and its application to model Pd electrodes for alcohols oxidation Pure and Applied Chemistry 96, 493-509(2024)
3) Capobianchi A., Imperatori P., Cannas C., Rusta N., Locardi F., Slimani S., Ferretti M., Peddis D., d'Acapito F., Tauanov Z., Laureti S., Varvaro G. - Extending the Pre-ordered Precursor Reduction strategy to L10 ternary alloys: the case of MnFePt Journal of Alloys and Compounds 1008, 176650-1-176650-9(2024)
4) d'Acapito F., Rehman M.A. - Effectiveness of ab initio molecular dynamics in simulating EXAFS spectra from layered systems Journal of Synchrotron Radiation 31, 1078-1083(2024)
5) De Amicis G., Testolin A., Cazzaniga C., d'Acapito F., Minguzzi A., Ghigna P., Vertova A. - In-situ surface activation of polycrystalline LaNiO3 electrocatalyst for the oxygen evolution reaction International Journal of Hydrogen Energy 87, 890-901(2024)
6) Ducka A., Blaszczak P., Zajac M., Mizera A., d'Acapito F., Bochentyn B. - Limited dissolution of transition metals in the nanocrystalline cerium (IV) oxide Ceramics International 50, 50921-50933(2024
7) Fantin A., Lepore G.O., Widom M., Kasatikov S., Manzoni A.M. - How atomic bonding plays the hardness behavior in the Al–Co–Cr–Cu–Fe–Ni high entropy family Small Science 4, 2300225-1-2300225-12(2024)
8) Fantin A., Manzoni A.M., Springer H., Kamachali R.D., Maass R. - Local lattice distortions and chemical short-range order in MoNbTaW Materials Research Letters 12, 346-354(2024)
9) Guerrini M., Magnaghi L.R., Fracchia M., Riccardi M.P., Pigoni G., Debbi G., Patrini M., Biesuz R., Tarantino S.C., Tamburini U.A., Ghigna P. - Minimizing the cobalt content in black ceramic pigments by Design of Experiments Ceramics International 50, 51181-51191(2024)
10) He X., Fracchia M., Coduri M., Scavini M., Ghigna P., Marelli M., Della Pergola R., Vertova A., Minguzzi A. - Structure and activity of carbonyl cluster-derived PtFe nanoparticles as electrocatalysts for the oxygen reduction reaction in alkaline media ACS Applied Energy Materials 7, 1561-1572(2024)
11) Maspero A., Bardelli F., Konidaris K.F., Uboldi M., Lucarelli C., Schiaroli N., Vitillo J.G. - Unraveling transfer hydrogenation mechanisms by ammonia borane to alkenes over self-healing copper nanoparticles: The complementary role of N-H bond, surface, and solvent ACS Catalysis 14, 9594-9606(2024)
12) Mirshokraee S.A., Muhyuddin M., Pianta N., Berretti E., Capozzoli L., Orsilli J., d'Acapito F., Viscardi R., Cosenza A., Atanassov P., Santoro C., Lavacchi A. - Ni-phthalocyanine derived electrocatalysts for oxygen reduction reaction and hydrogen evolution reaction: Active sites formation and electrocatalytic activity ACS Catalysis 14, 14524-14538(2024)
13) Morelli M.B., Caviglia M., Santini C., Del Gobbo J., Zeppa L., Del Bello F., Giorgioni G., Piergentili A., Quaglia W., Battocchio C., Bertelà F., Amatori S., Meneghini C., Iucci G.,

Venditti I., Dolmella A., Di Palma M., Pellei M. - Copper-based complexes with adamantane ring-conjugated bis(3,5-dimethyl-pyrazol-1-yl)acetate ligand as promising agents for the treatment of glioblastoma Journal of Medicinal Chemistry 67, 9662-9685(2024)
14) Muhyuddin M., Berretti E., Mirshokraee S.A., Orsilli J., Lorenzi R., Capozzoli L., d'Acapito F., Murphy E., Guo S., Atanassov P., Lavacchi A., Santoro C. - Formation of the active site structures during pyrolysis transformation of Fe-phthalocyanine into Fe-Nx-C electrocatalysts for the oxygen reduction reaction Applied Catalysis B: Environmental 343, 123515-123515-17(2024)
15) Ostroman I., Vallana N., Marchionna S., Gentile A., Ferrara C., Pellini I.C., Fracchia M., Pianta N., Ruffo R. - Oxidized Ti3Al(1-x)SnxC2 MAX phases as negative electrode materials for sodium ion batteries Journal of Power Sources 624, 235543-1-235543-12(2024)
16) Peerlings M.L.J., Han K., Longo A., Helfferich K.H., Ghiasi M., de Jongh P.E., Ngene P. - Synthesis and catalytic performance of bimetallic oxide-derived CuO–ZnO electrocatalysts for CO2 reduction ACS Catalysis 14, 10701-10711(2024)
17) Reale P., Pinto V., Cayado P., Celentano G., Armenio A.A., Rufoloni A., Santoni A., d'Acapito F. - Evidence of Gd substitution for Y in YBCO films with Gd excess Journal of Alloys and Compounds 983, 173921-1-173921-7(2024)
18) Riva L., Dotti A., Iucci G., Venditti I., Meneghini C., Corsi I., Khalakhan I., Nicastro G., Punta C., Battocchio C. - Silver nanoparticles supported onto TEMPO-oxidized cellulose nanofibers for promoting Cd2+ cation adsorption ACS Applied Nano Materials 7, 2401-2413(2024)
19) Romolini G., Sun L., Fron E., Acapito F., Grandjean D., Roeffaers M.B.J., Martin C., Hofkens J. - Single atom silver-phosphors in titanosilicate matrix for enhanced LED applications Advanced Optical Materials 12, 2301894-1-2301894-10(2024)
20) Russo R.E., Awais M., Fattobene M., Santoni E., Cavallera R., Zamponi S., Conti P., Berrettoni M., Giuli G. - Silver recovery from silicon solar cells waste by hydrometallurgical and electrochemical technique Environmental Technology & Innovation 36, 103803-1-103803-12(2024)
21) Sun L., Romolini G., Dieu B., Grandjean D., Keshavarz M., Fron E., d'Acapito F., Roeffaers M.B.J., Van der Auweraer M., Hofkens J. - Ultrasensitive luminescence switching of zeolite Y confined silver clusters for dual-channel oxygen sensing Advanced Optical Materials 12, 2400784-1-2400784-12(2024)
22) Virga S., Arrabito G., Ferrara V., Scopelliti M., Longo A., Pignataro B., Giannici F. - Bismuth drives the morphology and piezoresistivity of lead-free (TMSO)3Sn3xBi2(1−x)I9 halide perovskite thin films Journal of Materials Chemistry C 12, 12951-12961(2024)
23) Xue X., Asenbauer J., Eisenmann T., Lepore G.O., d'Acapito F., Xing S., Tübke J., Mullaliu A., Li Y., Geiger D., Biskupek J., Kaiser U., Steinle D., Birrozzi A., Bresser D. - Exploration of the lithium storage mechanism in monoclinic Nb2O5 as a function of the degree of lithiation Small Structures 5, 2300545-1-2300545-11(2024)

Contacts

Beamline responsible:
Francesco d'Acapito: dacapito@esrf.fr, +33 4 7688 2426, +33 6 8936 4302
Beamline scientists:
Alessandro Puri: puri@esrf.fr, +33 4 7688 2859
Jacopo Orsilli: jacopo.orsilli@esrf.fr, +33 4 7688 2530
Technical Services :
Fabrizio La Manna, lamanna@esrf.fr, +33 4 7688 2962

Beamline: +33 4 7688 2085
Laboratory: +33 4 7688 2743
Skype: LISA_beamline@EBS
Mattermost: @opd08

Web page: http://www.esrf.eu/UsersAndScience/Experiments/CRG/BM08/

Forthcoming proposals submission deadlines
ESRF quota: March 4th, 2025.
CERIC quota: early 2025, date to be announced.

Contributors to this issue

F. d'Acapito (CNR-IOM), J. Orsilli (Uni Mi Bicocca and CNR-IOM), A. Puri (Univ. Bologna and CNR-IOM), S. Amatori (Uni Roma Tre and CERIC), G. de Amicis and P. Ghigna (Univ. Pavia), X A. Minguzzi (Univ. Milano Statale), X. He (Univ. Milano Statale and Politecnico Milano), G. Romolini (K.U., Leuwen and U. Copenhagen), D. Grandjean (K.U., Leuwen), A. Fantin (BAM Institute, Berlin), C. Santoro (Univ. Mi Bicocca).